Preparation and spectroscopic properties of $Ca_2MgTeO_6:Tm^{3+}$ blue-emitting tellurate phosphors

Sumeng Jiang[1,2], Fanhua Zeng[1,2], Hui Liu[1,2], Yan Duan[1,2], and Bin Deng[1,2]*

[1]College of Chemistry＆Biology and Environmental Engineering, Xiangnan University, Chenzhou 423043, Hunan, P. R. China
[2]Hunan Provincial Key Laboratory of Xiangnan Rare-Precious Metals Compounds Research and Application, Chenzhou 423043, Hunan, P. R. China

Abstract. Various novel $Ca_2MgTeO_6:Tm^{3+}$ blue-emitting tellurate materials were synthesized via solid-state reaction. The structure and phase purity of prepared $Ca_2MgTeO_6:xTm^{3+}$ (x = 0.0025-0.10 mol) were examined by X-ray powder diffraction. The $Ca_2MgTeO_6:Tm^{3+}$ phosphors emit blue emission at 359 nm excitation. The optimum doping concentration was 0.02 mol. The concentration quenching mechanism in the Ca_2MgTeO_6 host was due to the electric dipole-dipole interaction. The The CIE chromaticity coordinates of $Ca_2MgTeO_6:Tm^{3+}$ phosphors located in the blue region. These results validated the $Ca_2MgTeO_6:Tm^{3+}$ tellurate phosphor can be used as good blue-emitting candidate for W-LEDs.

1 Introduction

White light-emitting diodes (W-LEDs), particularly phosphors-covered LEDs, have replaced traditional lighting sources (e.g., incandescent light, halogen tungsten lamp, and fluorescent lamp) owing to their energy conservation, long lifetime, high efficiency, and environment-friendly properties [1-5]. The common combination of commercial W-LEDs is that of blue InGaN chips and $Y_3Al_5O_{12}:Ce^{3+}$ yellow phosphors. Given the lack of a red component, this combination has a low rendering index and correlated color temperature (CCT). The other common method combines near-ultraviolet (n-UV) LED chips with trichromatic phosphors (yellow-, blue-, and red-emitting phosphors) [6-9]. It is imperative to fabricate a novel blue-emitting phosphor with effective absorption in the near-UV region.

There are many kinds of phosphors those have been reported. Rare-earth ions doped tellurates have arisen extensive interest due to excellent chemical and physical stability, such as $Li_3Gd_3Te_2O_{12}:Dy^{3+}$, $Ca_3TeO_6:Eu^{3+}$, and $NaLaCaTeO_6:Mn^{4+}$ [10-13]. Tm^{3+} is widely used as an efficient blue light emitting center , such as $CaHfO_3:Tm^{3+}$, $Li_3Gd_3Te_2O_{12}:Tm^{3+}$, $Ca_9NaGd_{2/3}(PO_4)_7:Tm^{3+}$, and $CaBi_4Ti_4O_{15}:Tm^{3+},Yb^{3+}$ many alternative Tm^{3+}-doped phosphors have been reported [14-17]. Ca_2MgTeO_6 ceramics were reported to a double perovskite family member and exhibited a monoclinic $P2_1/n$ structure [18]. Recently, $Ca_2MgTeO_6:Eu^{3+}$, $Ca_2MgTeO_6:Sm^{3+}$ phosphors emitted bright red/orange-emitting light under UV excitation [19, 20]. However, the Tm^{3+}-doped Ca_2MgTeO_6 phosphors had not been reported. In this work, Tm^{3+}-doped Ca_2MgTeO_6 blue-emitting phosphor has been synthesized by solid-state reaction. The powder X-ray diffraction (XRD), the photoluminescence excitation (PLE) properties, the photoluminescence emission (PL) spectra, and concentration quenching mechanism were investigated in depth.

2 Experimental section

The Ca2MgTeO6:xTm3+ powders were achieved through the solid-phase synthesis method. CaCO3 (analytical reagent), TeO2 (99.99%), (MgCO3)4·Mg(OH)2·5H2O (analytical reagent), Tm2O3 (99.99%), and Na2CO3 (analytical reagent). Na2CO3 was taken as charge compensation. They were fully mixed and ground in an agate mortar. Then, the mixture was calcined in air at 600℃ for one hour, and further sintered at 1100 °C for 24 h. Finally, after the muffle furnace cooled down to near room temperature, the products were ground for luminescence characterization. The structural properties of phosphor were measured by XRD through a Bruker D2 PHASER X-ray diffractometer with Cu Kα radiation source (λ = 0.15405 nm) operated at 40 kV with results between the range of 2θ = 15°−70°. The morphology was tested through scanning electron microscopy (JEOL, JSM-6490). The photoluminescence spectra and decay curves of the samples were characterized by the Edinburgh spectrometer (FLS 980).

3 Results and discussion

Fig. 1 presents the XRD patterns of Ca2(1-x)TmxNaxMgTeO6 (x = 0.0025, 0.005, 0.01, 0.02, 0.03, 0.05, and 0.10) phosphors. Obviously, with the increase

* Corresponding author: dengbinxnu@163.com(Bin Deng)

of Tm3+ dopant concentration, all the diffraction peaks were in accordance with the standard card (JCPDS no. 48-0108) of Ca2MgWO6 [21, 22]. It indicated that the small amount of Tm3+ ions does not evidently influence the crystal structure of Ca2MgTeO6. The ionic radii of the Ca2+ and Tm3+ ions are approximate corresponding to 1.12 Å and 0.994 Å (coordination number, CN = 8), respectively [23]. Apparently, a small amount of Ca2+ ions can be readily replaced by Tm3+ ions in the Ca2MgTeO6 host lattice. The as-prepared samples were with high phase purity.

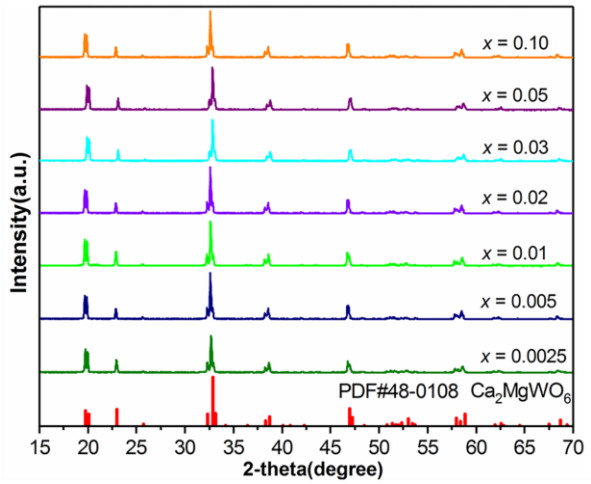

Fig. 1. XRD patterns of the $Ca_{2(1-x)}Tm_xNa_xMgTeO_6$ phosphors (x = 0.0025, 0.005, 0.01, 0.02, 0.03, 0.05, and 0.10).

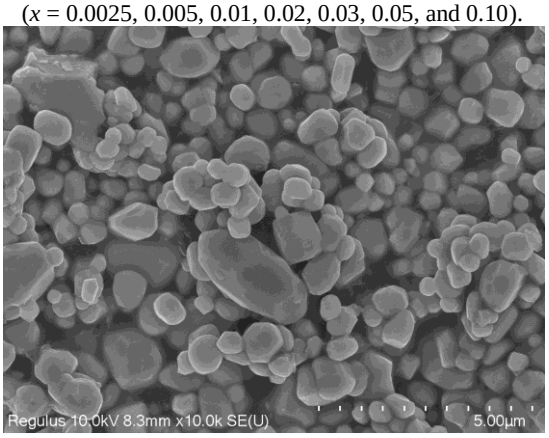

Fig. 2. Representative SEM micrograph of Ca_2MgTeO_6:0.02Tm^{3+}.

The morphology of the Ca2MgTeO6:0.02Tm3+ phosphor was characterized through scanning electron microscopy (SEM) and is shown in Fig. 2. The shapes of the particles are irregular and non-uniform, and some clusters are present. The existence of agglomerates is ascribed to high-temperature sintering. Particle size has a range of 1-2 μm.

The excitation spectrum of representative sample Ca2MgTeO6:0.02Tm3+ is monitored at 457 nm and shown in Fig. 3 curve (a). A broadband in the range of 200-250 nm related to O2-⟶Tm3+ charge transfer band [10]. Another peak in the excitation spectrum at 359 nm is assigned to the typical 4f–4f transition of 3H6→1D2 of Tm3+. Fig. 3 curve (b) displays the emission spectrum of Ca2MgTeO6:0.02Tm3+ at near-UV light λex = 359 nm. The main emission band at 457 nm due to the electronic dipole transition of 1D2 →3F4 of Tm3+ [15]. Importantly, the blue region's emission peaks suggested that Ca2MgTeO6:Tm3+ can be promising blue-emitting phosphors.

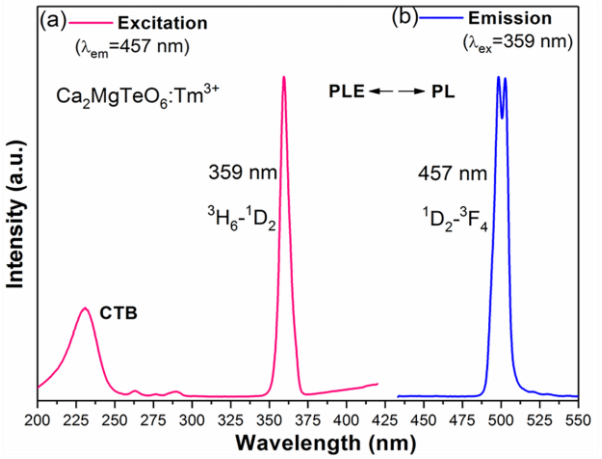

Fig. 3. Excitation spectrum (λ_{em} = 468 nm) and emission spectrum (λ_{ex} = 359 nm) of Ca_2MgTeO_6:0.02Tm^{3+} phosphor.

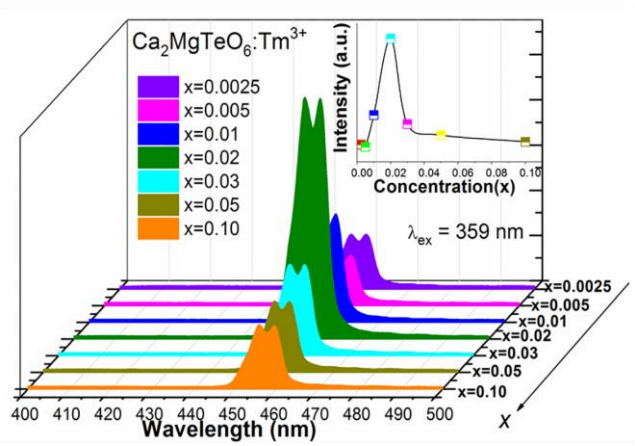

Fig. 4. The PL spectra (λ_{ex} = 359 nm) of $Ca_{2(1-x)}Tm_xNa_xMgTeO_6$ (x = 0.0025, 0.005, 0.01, 0.02, 0.03, 0.05, and 0.10) phosphors. The upper inset showed the influence of Tm^{3+} icon with different concentrations.

The PL spectra of Ca2(1-x)TmxNaxMgTeO6 (x = 0.0025, 0.005, 0.01, 0.02, 0.03, 0.05, and 0.10) phosphors as with different Tm3+ ions content are presented in Fig. 4. It is obvious that all the emission spectra have similar shape profiles with the increasing concentration. When the doping Tm3+ concentration in Ca2(1-x)TmxNaxMgTeO6 was x = 0.02 mol, the emission intensity of sample reached the most intense. Subsequently, exceeding 0.02 mol, the emission intensities of Tm3+ began to decrease gradually due to concentration quenching phenomena induced through the resonant energy transfer.

Blasse proposed the critical transfer distance (Rc) for analyzing the energy transfer mechanism, and the value can be estimated by this equation (1) [24, 25]:

$$R_c \approx 2\left(\frac{3V}{4\pi\ x_c N}\right)^{1/3} \quad (1)$$

here V (238.31 Å3) referred to the cell volume, Xc (0.02) represented the best doping concentration, and N (2) was the number of substitutable cations in a unit cell, the critical transfer distance Rc was estimated to be 22 Å,

much higher than that of exchange interaction distance (5.0 Å). Therefore, the electric multipole interactions between Tm3+ ions will be responsible for the concentration quenching phenomenon.

Furthermore, the following equation was used to evaluate the specific type of interaction mechanism in the energy transfer process of Tm3+ ions [26]:

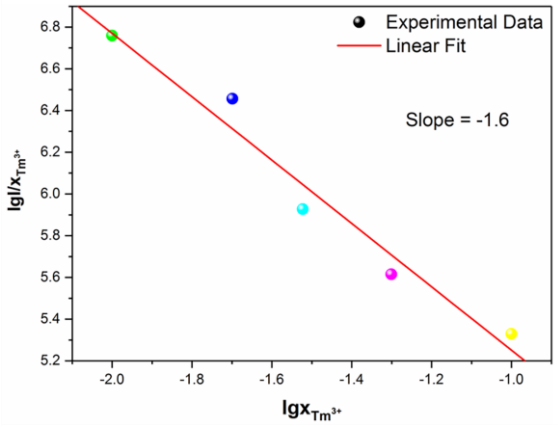

Fig. 5. Dependence of lg*x* on lg(*I*/*x*) of $Ca_2MgTeO_6:Tm^{3+}$ phosphors.

$$\frac{I}{x} = K\left[1+\beta\left(x\right)^{Q/3}\right]^{-1} \quad (2)$$

Here, Q is constant at 6, 8, and 10. They represent different energy transfer interactions, such as electric dipole-dipole (Q=6), dipole-quadrupole (Q=8), or quadrupole-quadrupole (Q=10) interactions, respectively. x stood for the activator concentration, K and β were constants at the same excitation condition [27]. Fig. 5 illustrates the linear plot. The slope parameter of the line was found to be −1.6. The Q value was fitted to 4.8, which approaches 6, indicating that the electric dipole-dipole interaction was the primary reason for the concentration quenching of Ca2MgTeO6:Tm3+ phosphors [28].

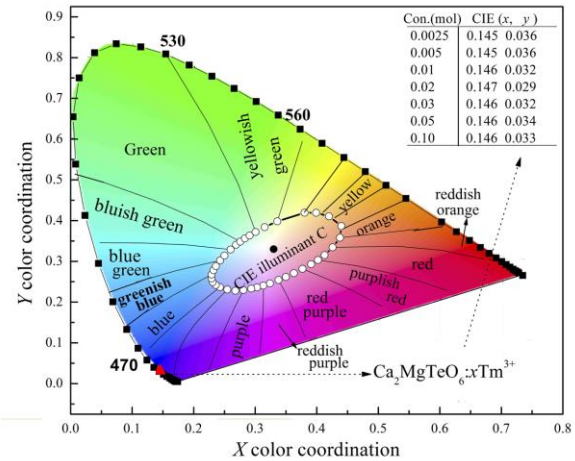

Fig. 6 The CIE chromaticity diagram $Ca_{2(1-x)}Tm_xNa_xMgTeO_6$ (*x* = 0.0025, 0.005, 0.01, 0.02, 0.03, 0.05, and 0.10) phosphors.

The CIE chromaticity coordinates are reasonable parameters for evaluating the performance of phosphor. Fig. 6 shows the CIE chromaticity diagram of Ca2(1-x)TmxNaxMgTeO6 (x = 0.0025, 0.005, 0.01, 0.02, 0.03, 0.05, and 0.10) phosphors. The chromaticity coordinates of Ca2MgTeO6:0.02Tm3+ are (0.147, 0.029). These Chromaticity coordinates are situated in the blue color region, Moreover, the color coordinates are all near the standard blue color coordinates.

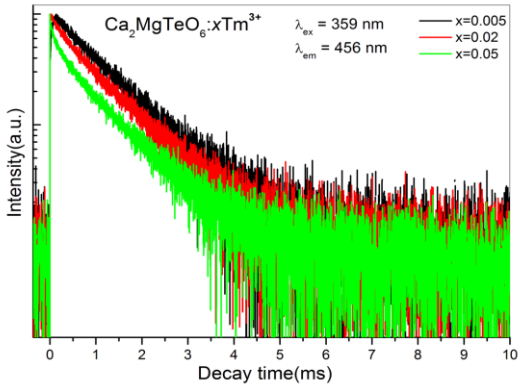

Fig. 7. Luminescence decay curves of $Ca_{2(1-x)}Tm_xNa_xMgTeO_6$ (*x* = 0.005, 0.02, and 0.05) phosphors.

Fig. 7 exhibits the luminescence decay lifetimes of Ca2(1-x)TmxNaxMgTeO6 (x = 0.005, 0.02, and 0.05) (λex = 359 nm, λem = 456 nm). The average decay lifetimes of Eu3+ ions are concluded by Equation (3) [29,30]:

$$\tau_m = \frac{\int_0^\infty t \times I_{(t)} dt}{\int_0^\infty I_{(t)} dt} \quad (3)$$

where I(t) is the luminescence intensity at t, and τm represents the value of lifetime. The decay lifetimes are calculated to be 1.007, 0.566, and 0.267 ms when the concentrations were 0.005, 0.02, and 0.05 mol, respectively. The decay time decreased with the enhancement of Tm3+ concentration. When the doping ion concentration of Tm3+ increases, the interaction between Tm3+-Tm3+ gradually strengthens, resulting in an increase in non-radiative transition possibility.

4 Conclusions

The Ca2MgTeO6:Tm3+ phosphors with different concentrations were successfully synthesized by the solid-state reaction method at 1100 °C for 24 h. Their phase purities were checked by XRD measurement. Particle size has a range of 1-2 μm. When excited at 359 nm, the Ca2MgTeO6:Tm3+ phosphors presented prominent emission peaks at 457 nm. The highest relative intensity was at 0.02 mol doping level. The concentration quenching was due to the electric dipole-dipole interaction. The critical distance related to concentration quenching to be 22 Å. The chromaticity coordinates of Ca2MgTeO6:0.02Tm3+ are (0.147, 0.029). The decay time of Ca2(1-x)TmxNaxMgTeO6 decreased with the increase of Tm3+ concentration. In conclusion, the Ca2MgTeO6:Tm3+ phosphor is a promising blue-emitting candidate for W-LEDs.

This project is financially supported by the Construction Program of the key discipline in Hunan Province, the Projects of the Education Department of Hunan Province (No.18A465), and Science and Technology Plan Project of Chenzhou city (jsyf2017014). The authors declare that there are no conflicts of interest related to this article.

References

1. L. Han, S. Xie, M. Wang, T. Sun, Q. Liu, G. Jiang, Y. Shi, Y. Tang, Mater. Lett. **234**, 241 (2019)
2. Y. Chen, X. Li, N. Li, Y. Quan, Y. Cheng, Y. Tang, Mater. Chem. Front. **3**, 867 (2019)
3. Q. Zhao, G.H. Tao, C.W. Ge, Y. Cai, Q.C. Qiao, X.P. Jia, Spectrosc. Lett. **51**, 216 (2018)
4. X. Zhang, N. Bao, X. Luo, S.-N. Ding, Biosens. Bioelectron. **114**, 44 (2018)
5. Y. Jin, C. Shi, X. Li, Y. Wang, F. Wang, M. Ge, Dyes Pigm. **139**, 693 (2017)
6. R. Yu, C. Wang, J. Chen, Y. Wu, H. Li, H. Ma, ECS J. Solid State Sci. Technol. **3**, R33 (2014)
7. G. Zhu, Y. Huang, C. Wang, L. Lu, T. Sun, M. Wang, Y. Tang, D. Shan, S. Wen, J. Zhu, Spectrochim. Acta, Part A **210**, 105 (2019)
8. D. Wang, X. Fan, S. Sun, S. Du, H. Li, J. Zhu, Y. Tang, M. Chang, Y. Xu, Sens. Actuators, B **264**, 304 (2018)
9. J. Shen, S. Shang, X. Chen, D. Wang, Y. Cai, Sens. Actuators, B **248**, 92 (2017)
10. S. Liu, J. He, Z. Wu, J.H. Jeong, B. Deng, R. Yu, J. Lumin. **200**, 164 (2018)
11. F. Fan, L. Zhao, Y. Shang, J. Liu, W. Chen, Y. Li, J. Lumin. **211**, 14 (2019)
12. K. Li, R. Van Deun, Chem. Commun. **55**, 10697 (2019)
13. H. Deng, Z. Gao, N. Xue, J.H. Jeong, R. Yu, J. Lumin. **192**, 684 (2017)
14. H. Fukushima, D. Nakauchi, T. Kato, N. Kawaguchi, T. Yanagida, Radiat. Meas. **133**, 106280 (2020)
15. B. Deng, C.S. Zhou, H. Liu, J. Chen, Mater. Sci. Forum **921**, 111 (2018)
16. B. Deng, J. Chen, C.-s. Zhou, H. Liu, Optik **202**, 163658 (2020)
17. T. Fu, X. Wang, H. Ye, Y. Li, X. Yao, J. Electron. Mater. **49**, 5047 (2020)
18. A. Dias, G. Subodh, M.T. Sebastian, M.M. Lage, R.L. Moreira, Chem. Mater. **20**, 4347 (2008)
19. L. Zhang, J. Che, Y. Ma, J. Wang, R. Kang, B. Deng, R. Yu, H. Geng, J. Lumin. **225**, 117374 (2020)
20. L. Zhang, Y. Xie, X. Geng, B. Deng, H. Geng, R. Yu, J. Lumin. **225**, 117365 (2020)
21. A. S.Y., F. N.F., A. I.F., Inorg. Mater. 921 (1975)
22. www.springermaterials.com/docs/VSP/summary/lpf-sd/00022668.html,
23. R.D. Shannon, Acta Crystallogr., Sect. A: Found. Crystallogr. **32**, 751 (1976)
24. G. Blasse, B.C. Grabmaier, Springer-Verlag, Berlin, Heidelberg 46 (1994)
25. W. Yang, C. Liu, S. Lu, J. Du, Q. Gao, R. Zhang, Y. Liu, C. Yang, J. Mater. Chem. C **6**, 290 (2018)
26. L.G. Van Uitert, J. Electrochem. Soc. **114**, 1048 (1967)
27. L. Tang, L. Zhou, X. Yan, K. Zhong, X. Gao, X. Liu, J. Li, Dyes Pigm. **182**, 108644 (2020)
28. L. Tang, L. Zhou, X. Yan, K. Zhong, X. Gao, J. Li, J. Photochem. Photobiol., A **387**, 112160 (2020)
29. L. Tang, J. Xia, K. Zhong, Y. Tang, X. Gao, J. Li, Dyes Pigm. **178**, 108379 (2020)
30. G. Zhang, L. Zhao, F. Fan, Y. Bai, B. Ouyang, W. Chen, Y. Li, L. Huang, Spectrochim. Acta, Part A **223**, 117343 (2019)